Dopamine induced switch in the subthreshold dynamics of the striatal cholinergic interneurons: A numerical study

Krisztina Szalisznyó, L. László Müller

www.elsevier.com/locate/yjtbi

Dopamine induced switch in the subthreshold dynamics of the striatal cholinergic interneurons: A numerical study

Krisztina Szalisznyó, László Müller

PII: S0022-5193(08)00485-2
DOI: doi:10.1016/j.jtbi.2008.09.029
Reference: YJTBI 5291

To appear in: *Journal of Theoretical Biology*

Received date: 18 March 2008
Revised date: 12 September 2008
Accepted date: 12 September 2008

Cite this article as: Krisztina Szalisznyó and László Müller, Dopamine induced switch in the subthreshold dynamics of the striatal cholinergic interneurons: A numerical study, *Journal of Theoretical Biology* (2008), doi:10.1016/j.jtbi.2008.09.029

Dopamine induced switch in the subthreshold dynamics of the striatal cholinergic interneurons: a numerical study

Krisztina Szalisznyó

Department of Biophysics, KFKI Research Institute for Particle and Nuclear Physics of the Hungarian Academy of Sciences P.O. Box 49, H-1525 Budapest, Hungary

László Müller

Department of Biophysics, KFKI Research Institute for Particle and Nuclear Physics of the Hungarian Academy of Sciences P.O. Box 49, H-1525 Budapest, Hungary

corresponding author: Krisztina Szalisznyó
Department of Biophysics,
KFKI Research Institute, RMKI
Hungarian Academy of Sciences,
H-1525 P.O. Box 49, Budapest, Hungary
Phone: +36 (1) 392-2222 (ext: 3257)
Fax: +36 (1) 392-2742
e-mail: szali@sunserv.kfki.hu

Preprint submitted to Elsevier *1 October 2008*

Abstract

Abstract

The striatum is a part of the basal ganglia, which are a group of nuclei in the brain associated with motor control, cognition and learning. Striatal cholinergic interneurons (AchNs) play a crucial role in these functions. AchNs are tonically active *in vivo* and *in vitro*, and are able to fire in the absence of synaptic inputs. AchNs respond to sensory stimuli and sensorimotor learning by transiently suppressing their firing activity. This pause is dopamine signal sensitive, but the neurophysiological mechanism of the dopaminergic influence is under debate. Both the regular spiking response as well as the pause response are influenced by the inwardly rectifying outward G_{kir}, a slow hyperpolarization activated noninactivating G_h, and calcium- and calcium dependent potassium conductances (Wilson and Goldberg, 2006), (Wilson, 2005). Recent experimental evidence has shown that dopaminergic modulations on G_h, G_{kir} and calcium conductances influence the AchN's excitability (Deng et al., 2007), (Aosaki et al., 1998). We employed computational models of the AchN to analyze the conductance based dopaminergic changes. We analyzed the robustness of these subthreshold oscillations and how they are affected by dopaminergic modulation. Our results predict that these conductances allow the dopamine to switch the AchN between stable oscillatory and fixed-point behaviors. The present approach and results show that dopamine receptors (D_1 and D_2) mediate opposing effects on this switch and therefore on the suprathreshold excitability as well. The switching effect of the dopaminergic signal is the major qualitative feature that can serve as a building block for higher network-level descriptions. To our knowledge this is the first paper that synthesizes the growing body of experimental literature about the dopaminergic modulation of the AchN-s into a modelling framework.

Key words: subthreshold oscillation; dopamine; striatum, cholinergic interneuron

Introduction

The striatal cholinergic interneurons (AchNs) are autonomous pacemakers (Pisani et al., 2007). They play a key role in the major functions of the basal ganglia including motor response selection and in motivational and reward-related behaviors. Dynamic imbalance between the dopaminergic inputs to the striatum and its intrinsic cholinergic innervation is believed to underlie the neuropathology of several neurological and psychiatric disorders (Pisani et al., 2007).

AchNs receive input from cortical and thalamic glutamatergic afferents (Wilson et al., 1998), and also from intrinsic striatal GABA-containing neuronal elements (DeBoer and Westerink, 1994). This local GABA-ergic system tonically inhibits the output of striatal AchNs via $GABA_A$ receptors (DeBoer and Westerink, 1994). AchNs are tonically active *in vivo* and respond to behaviorally salient stimuli. AchNs correspond to the tonically active neurons (TANs) of the primate striatum, which phasically decrease their discharge at the presentation of reward-related sensory stimuli (Ravel et al., 2006). Their responses consist of stereotyped phasic pauses of background activity, which is in some cases are preceded or followed by a transient increase of firing (Cragg, 2006).

This study seeks to better understand the autonomous subthreshold oscillatory behaviors of the AchNs, which do not depend on action potentials (Wilson, 2005), (Wilson and Goldberg, 2006). AchNs have three different pharmacologically separable subthreshold oscillatory mechanisms, each of which has a different time scale (Wilson and Goldberg, 2006):
I. The fastest oscillatory mechanism is persistent sodium current dependent and tetrodotoxin (TTX) sensitive. This subthreshold oscillation crucially depends on the removal of the calcium that entered the cell during action potentials (Wilson and Goldberg, 2006). **II.** The second oscillatory mechanism depends on two hyperpolarization activated conductances and does not require action potential generation. It is TTX and apamin insensitive (Wilson, 2005). This mechanism produces an intermediate frequency oscillation (1-5 Hz) in a subset of cholinergic interneurons, but it shapes and amplifies hyperpolarizations in all of them (Wilson and Goldberg, 2006), (Wilson, 2005). Thus the shape and the time-course of the characteristic hyperpolarized potentials (AHP) are influenced by these two hyperpolarization activated conductances (Wilson, 2005). **III.** Finally, the slowest oscillatory mechanism is generated by calcium currents and by the activation of a slow afterhyperpolarization (sAHP) mechanism (Wilson and Goldberg, 2006). These calcium currents are coupled to the calcium-dependent potassium currents, thereby creating mechanisms for control of the spontaneous firing patterns of the AchNs. They also account for the slow oscillations seen in a subset of cholinergic interneurons exhibiting rhythmic bursting. In all cholinergic interneurons, sAHP contributes to the slowdown in firing; sAHP may thus underlie the pause response of the AchNs *in vivo*.

Some AchNs exhibit all of these behaviours but typically only one dominates at a time. There is a complex interaction between these mechanisms allowing a cell to alternate between them (Wilson and Goldberg, 2006). These alternations are subject to neuromodulation (Wilson and Goldberg, 2006), but the factors determining

the relative dominance of each of these three subthreshold oscillations needs to be determined. Here, we have analyzed the **type II. and III.** oscillations, which do not depend on spiking activity.

Most AchNs express both D_2 and D_1 receptor types (Watanabe and Kimura, 1998). Dopaminergic actions on cholinergic interneurons are mediated through D_1 and D_2 receptors (Alcantara et al., 2003). Acetylcholine release is increased by D_1 agonists, while D_2 activation inhibits the acetylcholine release (Alcantara et al., 2003),(Damsma et al., 1990), (DeBoer and Abercrombie, 1996),(Exley and Cragg, 2007),(Cabrera-Vera et al., 2004),(Ding et al., 2006). We have summarized the experimental literature about the dopaminergic modulations of different AchN conductances in Table 1..

Dopaminergic modulatory effects on the AchN conductances

Destruction of dopaminergic inputs to the striatum abolishes the pause responses associated with stimuli used as signals for execution of learned movements, suggesting that the pause may be a response to dopaminergic input (Wilson, 2005). In neurons exhibiting regular firing *in vitro*, exogenous application of dopamine causes a prolongation of the depolarization-induced pause and an increase in the duration of slow afterhyperpolarization (sAHP) after depolarization (Bennett and Wilson, 1998).

A recent experimental study showed by partially blocking G_h with a specific blocker, that the AchN reduced firing and mimicked the effects of dopamine on sAHP (Deng et al., 2007). The G_h, being active at membrane potentials less than -50 mV, was inhibited by dopamine via activation of the D_2-like receptor (Deng et al., 2007). Consistently, D_2-like receptor agonist showed similar effects on sAHP and firing rate as those induced by an G_h channel blocker (Deng et al., 2007). Application of dopamine reversibly inhibited G_h in a dose-dependent manner, and caused a hyperpolarizing shift in the voltage dependent activation of G_h, of about -6 mV (Deng et al., 2007). Dopamine has a twofold effect through D_2 receptors on the AchN-s. First, there is a partial direct inhibition of G_h (Deng et al., 2007). Secondly, dopamine causes hyperpolarizing shift of the Boltzmann-function of the G_h, which also contributes to the dopamine induced reduction of this current through D_2 receptors (Deng et al., 2007).

Another experimental study demonstrated that dopamine depolarizes the AchN-s by a D_1-mediated suppression of resting K^+ conductance (Aosaki et al., 1998). This K^+ conductance is hyperpolarization activated and Ba^{2+} sensitive, thus it is most likely the inwardly rectifying outward conductance G_{kir} (Aosaki et al., 1998). The same study demonstrated another dopaminergic D_1-mediated effect, and this is the opening of a nonselective cation channel (Aosaki et al., 1998). The reversal potential of this current is around $-40mV$, which makes it likely, that this is the G_h conductance (Aosaki et al., 1998). Endogenous dopamine facilitates striatal *in vivo* acetylcholine release by acting on D_1 receptors localized in the striatum (Consolo et al., 1992). Furthermore dopamine is important to maintain the muscarinic M_4 receptor signalling (Ding et al., 2006),(Calabresi et al., 1998). M_4 receptors activate a

Ba^{2+} sensitive K^+ conductance that is most probably attributable to $Kir3$ channels (Ding et al., 2006),(Calabresi et al., 1998). Dopamine depletion downregulates the M_4 receptor mediated $Kir3$ channel activation (Ding et al., 2006),(Calabresi et al., 1998). Furthermore, it has been shown that dopamine mediated prolongation of the characteristic pauses of the AchN might be attributable to regulations on the recovery of AHP-s (Deng et al., 2007). Another experimental study demonstrated D_1 receptor mediated enhancement of the afterhyperpolarization (Bennett and Wilson, 1998). The pharmacological blockade of I_{kir} nearly abolished the afterhyperpolarization, although the AHP current was almost unaltered (Wilson, 2005).

AchN-s express a heterogeneous population of Ca^{2+} channels, among them Q-,N-,L-,P- and R-type Ca^{2+} channels (Yan et al., 1997). N- and L-type currents constitute the largest fraction of the Ca^{2+} currents in these neurons (Yan and Surmeier, 1996) and low voltage activated Ca^{2+} channels are not seen (Yan and Surmeier, 1996). D_2 receptor signalling reduces the Ach release from the AchN terminals by modulating voltage gated $Ca_v.2$ (N-type) Ca^{2+} channels, and thus this signalling pathway contributes to the ability of D_2 receptors to reduce striatal acetylcholine release (Yan et al., 1997), (Pisani et al., 2000). On the other hand stimulus-evoked dopamine release influences spike timing via D_1 receptor- mediated enhancement of the AHP and this is most likely mediated by L-type Ca^{2+} current (Bennett and Wilson, 1998).

Given this background, we synthesized the subthreshold mechanisms linking dopamine and the alteration in the AchN activity, and followed and analyzed the computational consequences of these alterations mediated by D_1 and D_2 receptors.

Methods: subthreshold dynamics of the AchN model

Medium frequency oscillation

In this study we first analyzed the intermediate frequency subthreshold oscillation of the AchN-s in detail (Wilson, 2005). We reproduced the intermediate frequency subthreshold oscillation with a point neuron model by two hyperpolarization activated conductances and a leak conductance (Wilson, 2005). The subthreshold dynamics of the model is governed by the following equations (Wilson, 2005), (Izhikevich, 2002):

$$C\frac{dV}{dt} = -I_h - I_{kir} - I_{leak} + I_{inj}. \tag{1}$$

The slow I_h current is governed by the following equations:

$$I_h = G_h(V - E_h), \tag{2}$$

where

$$G_h = \overline{g_h} h. \tag{3}$$

The differential equation for the h gating variable is the following:

$$\tau_h \frac{dh}{dt} = \frac{1}{1 + exp\left(\frac{V - V_{(1/2)h}}{V_{(s)h}}\right)} - h. \tag{4}$$

The very fast I_{kir} current is described as:

$$I_{kir} = G_{kir}(V - E_K), \tag{5}$$

where G_{kir} stands for the fast inwardly rectifying outward K^+ conductance. The G_{kir} conductance is assumed to be voltage dependent, but not time dependent; since it acts quickly the time dependence is assumed to be negligible (Wilson, 2005), (Wessel et al., 1996):

$$G_{kir} = \frac{\overline{g_{kir}}}{1 + \exp\left(\frac{V - V_{(1/2)kir}}{V_{(s)kir}}\right)}. \tag{6}$$

In one set of simulations we used voltage dependent τ_h. Since the channel kinetics for this conductance in AchN-s have not been described in the literature, the voltage dependent τ_h was borrowed from a study describing a conductance from the thalamic relay neurons (Huguenard and McCormick, 1992).

$$\tau_h = \frac{1}{exp(-14.59 - 0.086V) + exp(-1.87 + 0.0701V)} \tag{7}$$

In other set of simulations we considered constant, voltage independent τ_h values, according to a recent modelling study (Wilson, 2005).

The leak conductance I_{leak} is described as:

$$I_{leak} = \overline{g_l}(V - E_l). \tag{8}$$

The parameters used in this study are shown in Table 2.

Low frequency oscillation

We analyzed the very low frequency Ca^{2+} dependent subthreshold oscillation of the AchN-s in detail, while implementing an earlier phenomenological model (Wilson and Goldberg, 2006). We examined the effect of the dopaminergic modulation on this oscillation (Bennett and Wilson, 1998). The very slow frequency oscillation is dependent on the $G_{Ca_v.1}$ (L-type) calcium conductance and dopamine modulates (increases) this conductance most likely via D_1 receptors (Bennett and Wilson, 1998). We have made a slight modification on the earlier model, in order to reproduce the very low frequency oscillation (Wilson and Goldberg, 2006). The subthreshold dynamics of this model is governed by the following three differential equations (Wilson and Goldberg, 2006):

$$C\frac{dV}{dt} = -I_{Ca} - I_{sAHP} - I_{leak} - I_{Kv}, \tag{9}$$

where V is the membrane potential. CaB denotes the proportion of sAHP channel related Ca^{2+} binding sites that have bound calcium. The dynamics of this variable governed by:

$$\frac{dCaB}{dt} = \alpha[Ca](1 - CaB) - \beta(CaB). \tag{10}$$

The intracellular calcium concentration has the following dynamics:

$$\frac{d[Ca]}{dt} = \frac{buf}{d/6}\left(\frac{-I_{Ca}}{zF} - \frac{[Ca]}{\tau_{Ca}}\right). \tag{11}$$

The $[Ca]$ is the concentration of the free calcium, buf is the proportion of free to total intracellular calcium. The slow afterhyperpolarizing current is described by the following equation:

$$I_{sAHP} = \overline{g_{sAHP}}(CaB)^4(V - V_K). \tag{12}$$

The voltage sensitive Ca^{2+} current is described as:

$$I_{Ca} = \frac{\overline{g_{Ca}}}{1 + exp\left(-\frac{V - V_{(1/2)Ca}}{V_{(s)Ca}}\right)}(V - V_{Ca}). \tag{13}$$

The voltage-sensitive potassium current is governed by:

$$I_{Kv} = \frac{\overline{g_{Kv}}}{1 + exp\Big(-\frac{V - V_{(1/2)Kv}}{V_{(s)Kv}}\Big)}(V - V_K). \quad (14)$$

The leak current is described by the following equation:

$$I_{leak} = \overline{g_{leak}}(V - V_{leak}). \quad (15)$$

The parameters which were used while reproducing the very low frequency oscillation are listed in Table 3. (Wilson and Goldberg, 2006): We have changed τ_{Ca} and $\overline{g}_{Ca}$ compared with the earlier model (Wilson and Goldberg, 2006).

Numerics

Simulations were performed on a SUN Ultra-4 station running the Debian Linux operating system (kernel version 2. 0. 34) using XPP simulation software (version 5.91). The differential equations were solved using the 4th order Runge-Kutta method, with a step size of 0.05 msec. For the bifurcation analysis the AUTO module of XPP was used. We have checked our analytic results with Maple software.

Results

We have modelled two types of subthreshold autonomous oscillation of the AchN: the medium and the low frequency oscillations (Wilson and Goldberg, 2006). We analyzed the medium frequency oscillation by incorporating two hyperpolarization activated conductances in the point neuron model (Wilson, 2005). We were able to reproduce the medium frequency autonomous subthreshold oscillations based solely on the G_{kir}, G_h and the leak conductances (Fig.1.A.B.) (Wilson and Goldberg, 2006), (Wilson, 2005), (Izhikevich, 2002). Secondly, we modelled the very low frequency, Ca^{2+} dependent oscillation (Wilson and Goldberg, 2006). The dopaminergic modulation on different conductances were analyzed, according to the experimental literature. We followed the sensitivity of the subthreshold behavior on several model parameters, including those which are known to be altered by dopamine (Deng et al., 2007), (Aosaki et al., 1998).

Dopaminergic effect on the G_h

We have found that by decreasing the $\overline{g_h}$ value the amplitude of the subthreshold oscillation does not change (Fig.2.A.). A recent experimental study demonstrated that activation of the D_2 receptors had no effect on the AHP amplitude (Deng et al., 2007), which is in agreement with our simulation results (Fig.2.A.). Decreasing the $\overline{g_h}$ value even further, the model stops exhibiting periodic oscillatory solution

(Fig.2.A.). Decreasing the $\overline{g_h}$ value in the physiologically plausible range (Wilson, 2005), the frequency of the subthreshold oscillation is a non-monotonic function (Fig.2.B.). The modeling results predict that dopaminergic modulation (lowering the $\overline{g_h}$ from 2 $\frac{\text{mS}}{\text{cm}^2}$) causes a drop in the subthreshold oscillation frequency. Experimental data have shown, that partial blockade of G_h is sufficient to decrease the firing rate in the AchN (Deng et al., 2007). The simulation results presented here are compatible with the experimental findings, since in case of higher frequency subthreshold oscillations the firing threshold is probably reached more times, than when the subthreshold oscillation is slower (Fig.2.B.). The effect of D_1 receptor mediated increase was also modelled. We found that again, the amplitude and the peak values of the subthreshold oscillations did not change (Fig.2.A.), but the frequency - again due to the non-monotonicity - slightly decreased (Fig.2.B.).

We also looked at the dynamic regime with two different $\overline{g_h}$ values, while keeping the $\overline{g_{kir}}$ fixed (Fig.2.C.D.). Throughout this study, the dynamic range (or dynamic regime or width) refers to the range of injected currents bounded by where the model neuron starts to exhibit subthreshold oscillation and where it stops oscillating. Lower $\overline{g_h}$ value resulted in lower membrane potential at the injected current values, where the model started to exhibit subthreshold periodic solutions (Fig.2.C.). Although the amplitudes of the periodic solutions do not show significant differences with the two $\overline{g_h}$ at a certain injected current value, the frequencies reach lower values with lower $\overline{g_h}$-s (Fig.2.D.). This is again in agreement with the experimental observations of dopamine induced firing rate drop in AchN-s (Deng et al., 2007). It should be noted that the stable periodic solution (subthreshold oscillation) emerges via supercritical Hopf bifurcation as we increase the injected current parameter (Fig.2.C.D.). When we lowered the G_h significantly ($\overline{g_h} = 1\ \frac{\text{mS}}{\text{cm}^2}$), in a very narrow parameter regime a stable periodic solution emerges with very steeply decreasing frequency (Fig.2.D.). However, though the model predicts this very narrow parameter regime, due to the lack of experimental evidence we do not consider this phenomena as physiologically plausible (Fig.3.B.).

We have found that even though the two half activation voltages of the Boltzmann-functions are the same for the G_{kir} and the G_h, the difference between the time constants (one being instantaneous and the other is very slow) and the fact that G_{kir} is amplifying while the G_h is resonant is sufficient for the subthreshold excitability (Fig.3.A.) (Izhikevich, 2002). The amplifying and resonant property is dependent on the operating voltage range relative to the reversal potential ($V - E_{ion}$) (Izhikevich, 2002), (Mao et al., 2003) (Fig.3.A.). Since dopamine shifts the $V_{(1/2)h}$ into more hyperpolarized regime, (thus the relative position of the half activation voltage values is changing), we next examined the consequences of the dopamine induced Boltzmann-function shift (Deng et al., 2007). We have found that the dopamine induced shift in the half activation voltage value does not change significantly the amplitude, or the frequency of the subthreshold oscillation in the spontaneously firing neuron model ($I_{inj} = 0\ \frac{\mu\text{A}}{\text{cm}^2}$) (Fig.4.A.B.).
However, it does change the dynamic range. The shift induces a hyperpolarization (Fig.4.C.) and the subthreshold oscillation emerges with higher injected current values (Fig.4.C.). On the other hand, the periodic solution survives to higher injected current values (Fig.4.C.). At higher $V_{(1/2)h}$ values (without dopamine) the

subthreshold oscillation reaches higher frequencies in the hyperpolarized regime, which is again in correspondence with the experimental results (Fig.4.D.) (Deng et al., 2007).

The effect of dopaminergic modulation suggests that the membrane became less excitable but exhibited periodic slow oscillation in larger current injection parameter values as well (Fig.4.D.). Again, we have found that with decreased $V_{(1/2)h}$ value in a very narrow injected current parameter regime a stable periodic solution emerges with steeply decreasing frequency (Fig.4.D.). Until experimental studies demonstrate evidence of this phenomena, we consider this very narrow regime as physiologically unrealistic (Fig.4.D.).

Effect of the G_h's time constant

G_h has an activation time constant of about 385 msec when it is evoked with a hyperpolarizing step of -90 mV and deactivation time constant of 237 msec when measured at -70 mV after a hyperpolarization of -150 mV (Deng et al., 2007). We have used a parameter set from a recent modeling study, where the τ_h was chosen to be 300 msec (not voltage dependent), because it was sufficient to reproduce the physiologically plausible subthreshold oscillation (Wilson, 2005). Dopamine significantly enhances the G_h in several systems by accelerating its time constant (τ_h), and enhances its maximal conductance $\overline{g_h}$ (Peck et al., 2006). Therefore we examined the effect of changing the τ_h (where the τ_h was voltage independent). We have found, that the varying τ_h does not influence much the amplitude and the peak membrane potential value in any of the injected current value in the physiological range, but it slightly increases the frequency of the subthreshold oscillations (Fig.5.A.B.). These simulation results suggest, that dopamine modulated G_h may play a role in determining the frequency of the subthreshold oscillation (Deng et al., 2007). Long lasting hyperpolarizing currents (simulated with step currents) increase the firing frequency but decrease the amplitude and the peak voltage value of the subthreshold oscillation (Fig.5.A.B.)

Effect of the dopaminergic modulation on the G_{kir}

We implemented the dopaminergic modulation of the inwardly rectifying outward G_{kir} according to the experimental evidence (Aosaki et al., 1998),(Ding et al., 2006),(Calabresi et al., 1998),(Bennett and Wilson, 1998) (Table 1.).

First we looked at the effects of the decreasing G_{kir} conductance on the amplitude and the frequency of the subthreshold oscillation in the point neuron model (Aosaki et al., 1998). Lower $\overline{g_{kir}}$ values (coherent with the dopaminergic modulation (Aosaki et al., 1998)) resulted in lower peak voltage values (Fig.6.A.). The $\overline{g_{kir}}$/firing frequency function is non-monotonic (Fig.6.B.). When we considered increasing $\overline{g_{kir}}$ values (Ding et al., 2006), we observed higher peak values (Fig.6.B.), but nonmonotonic $\overline{g_{kir}}$/firing frequency function (Fig.6.B.).

We next examined the subthreshold excitability by changing the injected current value, and looking at the bifurcation curves with two different $\overline{g_{kir}}$ values (Fig.6.C.D.). We have found, that with a higher $\overline{g_{kir}}$ value the stable periodic solution appears at higher injected current, and the amplitude and the peak value of the subthreshold oscillation is higher (Fig.6.C.). The periodic stable solution disappears with higher injected current values (Fig.6.C.). On the other hand, the physiologically plausible $\overline{g_{kir}}$ value leads to higher frequency oscillations in a more hyperpolarized regime, than in case of a model with higher $\overline{g_{kir}}$ values (Fig.6.D.). In a depolarized regime the model with larger $\overline{g_{kir}}$ still exhibits periodic solution, while the one with lower $\overline{g_{kir}}$ already stopped oscillating (Fig.6.D.).

These simulation results have two implications: First, as was found in case of the G_h modulation, the dopaminergic effects resulted in a slightly lower frequency of the subthreshold oscillation (again, this is due to the non-monotonicity), which probably causes lower probability of spike threshold crossing. This is in good agreement with the experimental findings, and we have found it with both increasing and decreasing the $\overline{g_{kir}}$ conductance. Secondly we have found that the dopamine increases the amplitude (the peak potential value) of the subthreshold oscillation, resulting in a dopamine induced decreased suprathreshold excitability through D_1 (Aosaki et al., 1998), but increasing it via M_4 receptor mediated $Kir3$ channel activation (Ding et al., 2006),(Calabresi et al., 1998). Therefore we conclude that the two effects of the dopamine modulated G_{kir} are opposing on the amplitude of the medium frequency subthreshold oscillation, but on the frequency they have similar effects.

Two dimensional analysis of the dopaminergic effect in the medium frequency subthreshold oscillation

We examined the effects of the dopamine induced maximal conductance changes of the I_h and I_{kir} in a two dimensional representation (Fig.7.). With this approach, we explored the width of the parameter regimes, where the model exhibited subthreshold autonomous oscillations. We obtained the 2D bifurcation diagrams numerically, and analytically as well (Appendix) (Fig.7.A). The two dimensional representation of the D_1 receptor mediated effect shows, that dopamine depletion moves the physiologically realistic model (Wilson, 2005) to the regime, where the model exhibits periodic stable solution in the subthreshold regime (with the model, where zero injected current was applied) (Fig.7.A.). The model predicts, that the D_1 receptor mediated effects are able to move the model into the stable fixed point regime, and dopamine depletion has an abrupt effect. Thus even a slight change in the dopaminergic modulations moves the model into the oscillatory regime.

Lowering the dopaminergic D_1 effect, the depletion will shift the neuron into a slightly lower frequencies (Fig.7.B.) in the subthreshold oscillatory regime, but the peak value of the subthreshold oscillation becomes slightly higher (Fig.7.C.). On the other hand the D_2 receptor mediated effect together with the M_4 receptor mediated $Kir3$ channel activation have opposing effects: Dopamine moves the cell into the oscillatory regime, while depleted states will push the cell abruptly to the stable fixed

point regime (Fig.7.B.C.), where the medium frequency subthreshold oscillation vanishes. In summary, the simulation results suggest that the dopamine and likewise the dopamine depletion are acting on two different and opposing receptor systems, one which moves the neuron out, the other which pushes the neuron into the stable periodic oscillatory regime.

Experimental results suggest that dopamine depletion results in higher firing frequency (thus increased striatal acetylcholine release) and less regularity in the firing of the AchN-s (Deng et al., 2007),(Fino et al., 2007),(Ding et al., 2006). In contrast, dopamine causes a reduction in striatal cholinergic interneuron activity seen in the initial stages of associative learning and movement planning, but causes an increase of regularity (CV) in the interspike intervals (Deng et al., 2007). Our modeling results support the experimental findings that the D_2 and M_4 receptor mediated effects are the dominant in the AchN-s (over the D_1) (Ding et al., 2000).

In dopamine depleted states the medium frequency subthreshold oscillation has higher frequency (Fig.7.B) with slightly lower peak amplitude (Fig.7.C). Further depletion moves the model into stable fixed point regime, suggesting that the spike generating mechanism causes a more excitable membrane [when the G_h and G_{kir} mediated subthreshold oscillation is less prominent or absent, thus there is a fixed point solution]. On the other hand the dopaminergic (D_2) modulation of the above subthreshold conductances slows down the subthreshold oscillation, resulting in a decreased suprathreshold excitability but more regularity in spiking (Deng et al., 2007). This seems to be in agreement with the dopamine induced lower frequency of the subthreshold oscillation (Fig.7.B.). Therefore it is most likely, that the regularity of the AchN firing decreases in dopamine depleted states when the slower autonomous subthreshold oscillation does not influence the suprathreshold fast spike-generating dynamics. On the other hand dopamine modulates the subthreshold conductances such that they are able to govern the suprathreshold spike generating machinery with lower frequency but more regularity (Deng et al., 2007).

Amplification of synaptic events by the hyperpolarization-activated conductances

Although synaptic inputs clearly influence spike timing in AchN-s, the characteristic spike sequences are very much influenced by the intrinsic membrane properties (Wilson, 2005), (Wilson and Goldberg, 2006). Dopamine mediated enhancement of the afterhyperpolarization may be directly responsible for the pause at the early phase of task acquisition (Bennett and Wilson, 1998). Therefore revealing the dynamics of the interaction between synaptic perturbation and intrinsic excitability will lead to better understanding of the striatum. In what follows we examined the amplification of the synaptic potentials by the two hyperpolarization activated conductances in the point neuron model, which are responsible for the medium frequency subthreshold oscillation.

An experimental and modelling study suggested that AchN neurons' pause response

is an intrinsically amplified hyperpolarizing synaptic event. Thus the pause is not a graded response to the sum of hyperpolarizing events (Wilson, 2005). The AchN-s exhibit spontaneous subthreshold oscillations without any additional current (positive or negative) injection, which was reproduced in this modelling study (Wilson, 2005). While injecting hyperpolarizing currents, there are two parameter regimes, where the model exhibits stable fixed point solution (on Fig.3.B. regime I. and III.). In this differential equation system the hyperpolarizing events could only be amplified by the G_{kir} conductance. The equilibrium potential of the I_h is at -40 mV (Wilson, 2005), therefore the hyperpolarizing events are dampened by this current (Fig.3.B.). On the other hand both G_{kir} and G_h cause input resistance decrease to hyperpolarizing directions (Fig.3.A.), thus both dampen the synaptic events' amplitude through decreasing the input resistance.

We examined the effect of the G_{kir} on the amplification and found that it has the following two counteracting effects: First, it decreases the input resistance in hyperpolarized membrane potential regimes, as in the case of the G_h conductance. Secondly, it amplifies the hyperpolarizing membrane potential changes, due to its -90 mV reversal potential. The amplification of the hyperpolarizing synaptic events was examined in three different injected current regimes (Regimes I., II., III. on Fig.3.B.). If the synaptic events (EPSC, IPSC) have small amplitudes where the model (and the AchN neuron) exhibit stable fixed point solutions, then the active conductance mediated change on the synaptic voltage amplitude can be approximated by the I/V curve change, which is induced by the active conductance (Szalisznyó, 2006).

Two sets of simulation results were compared: one which was adjusted to reproduce the physiologically plausible subthreshold oscillation properties (Wilson, 2005) and the second, where the $\overline{g_{kir}}$ value was decreased (Fig.3.B.). In *regime I.*, the input resistance decrease mediated change dominates. Thus the slope of the I/V curve with less $\overline{g_{kir}}$ value is steeper than the one with higher $\overline{g_{kir}}$ (Fig.3.B.). On the contrary in *regime III.*, the G_{kir} mediated hyperpolarizing effect dominates. Thus larger $\overline{g_{kir}}$ values result in steeper I/V curves (Fig.3.B.). This later result is partly due to the larger battery term of the I_{kir} current in a more depolarized *regime III.*, than in *regime I.*, and also because the I_h is less activated in *regime III.* than in *regime I.* and thus does not contribute to the input resistance significantly.

Phase dependency of the delay in the subthreshold oscillation evoked by IPSPs and EPSPs

A detailed experimental *in vitro* study examined the ability and precision with which EPSPs and IPSPs influence action potential timing in the AchN-s (Bennett and Wilson, 1998). In those experiments regular spiking was induced by injecting small amplitude depolarizing current (Bennett and Wilson, 1998). The subthreshold oscillation has a strong influence on spike generation by moving the membrane potential towards and away from the firing threshold. Therefore, we next studied the time-varying solutions of the parameter regime, where the model exhibits stable periodic solutions (*regime II.* on Fig.3.B.).

In the experiments, the sub- and the suprathreshold conductances influence the ability of the brief current injections to delay or to advance the spike generation. Our motivation was to determine, to what extent could the subthreshold oscillation generating conductances account for the results seen *in vitro* (Bennett and Wilson, 1998), and also to quantify the intrinsic amplification of the hyperpolarizing events (Wilson, 2005). Depolarizing and hyperpolarizing step currents were applied for short duration (50 msec, 0.5 μA/cm^2) at different phases of the subthreshold membrane oscillation (Fig.8.A.).

We considered the phase beginning from the most depolarized state until the consecutive next in a simulation where there was no additional current pulse applied (Fig.8.A.B.). From certain aspects the question is posed similarly, as it is in case of phase response curves, except that the phase is determined between two most depolarized states, thus the "excitability" is in the subthreshold regime (Fig.8.A.B.). Although there is no spike generating process implemented in this model, the spike generation is most likely when the neuron (and our model) reaches higher membrane potentials during the subthreshold oscillation.

Therefore we also used the interspike interval (ISI) nomenclature, and here it refers to the time period which is between the two consecutive most depolarized membrane potential values within a period (Fig.8.A.B.). In case of phase response curves the transient change in the cycle period of an oscillator is induced by a small amplitude and short perturbation. We were motivated by the experimental results, which were designed to explore the EPSP/IPSP amplitude change as a function of the phase at which they were received (Bennett and Wilson, 1998). Therefore we applied currents which were higher in amplitude and longer in duration, than in a classic phase response methodology.

Effect of depolarizing current injection steps

It was demonstrated experimentally that intrastriatal stimulation evoked EPSPs produced a phase-dependent effect in the interspike intervals (ISIs) duration in the AchN-s (Bennett and Wilson, 1998). In the experiments the ability of the depolarizing inputs (EPSPs) arriving during the first-third of the ISI to influence the spike timing is very low: it practically did not effect the spike timing (Bennett and Wilson, 1998). The simulation results presented here are consistent with these experimental observations, because the first third of the ISI does not induce phase delay or advance in the subthreshold oscillation (Fig.8.C.). Our results predict a short and small amplitude advance (shortening of the ISI) followed by more prominent phase delay (prolonging of the ISI) (Fig.8.C.).

Experimental observations showed that intrastriatal stimulation produces bi-phasic effect on the spike timing: EPSP-s that were evoked before the first spike caused an increase on the subsequent ISI, whereas EPSPs evoked late in the ISI shortened the time between spikes (Bennett and Wilson, 1998). Our modelling analysis revealed similar bi-phasic results. The difference was that in our simulations the phase delay followed by the advance was approximately in the last third of the ISI, whereas in the experiments it was more in the middle of the cycle (Fig.8.C.) (Bennett and Wilson, 1998).

Our results predict, that the two hyperpolarization activated conductances are sufficient to reproduce and contribute to the experimental observations even without considering the spike generating conductances. Furthermore our simulation results were sufficient to explain the experimental observation of the phase-dependent increase in the EPSP amplitude during the ISI as well (Fig.8.D.) (Bennett and Wilson, 1998). The only difference between our findings and the experimental results is that the depolarizing current injections which arrived in the last part of the ISI were not amplified. This is due to the autonomous oscillation driven rapid membrane potential increase of the last part of the cycle (Fig.8.A.D.).

The same experimental study suggested that D_1 receptor mediated enhancement of the AHP explains the paradoxical effect of the EPSPs to cause a prolongation in the ISI, when evoked before or shortly after the spike (Bennett and Wilson, 1998). Our modeling study revealed similar results, thus we suggest an alternative explanation which is the interplay between the two hyperpolarization activated conductances. Although our simulation results were in agreement with the experimental findings and are thus sufficient to explain these observations, it is also possible that the hyperpolarization activated conductances act in concert with the D_1 receptor mediated effects (Bennett and Wilson, 1998) (Fig.8.C.D.).

Effect of hyperpolarizing current injection steps

It was demonstrated experimentally that in contrast to EPSPs, the IPSPs produced a phase-independent effect in the interspike intervals (ISIs) duration (Bennett and Wilson, 1998). The same experimental study revealed differences between an IPSP evoked by intrastriatal stimulation and direct hyperpolarizing current injection (Bennett and Wilson, 1998). The intrastriatal IPSPs (after a pharmacological blockade of AMPA and NMDA receptors) evoked a prolongation of the ISI (delay) irrespective of when they were evoked (Bennett and Wilson, 1998). In contrast to the synaptic IPSPs, the brief hyperpolarizations evoked by current injection had a phase-dependent effect, but the response was not bi-phasic, thus they only produced phase dependent prolongation (delay) of the ISI. The later the hyperpolarizing current was applied after a spike, the longer delay it caused in the timing of the subsequent spike (Bennett and Wilson, 1998).

We used an analogous simulation protocol to that is described for EPSPs above. Our results are only in a partial agreement with the experimental observations. The model showed bi-phasic phase response curve to hyperpolarizing current injections (Fig.8.E.). The phase delay dominates in the first third of the cycle, and when the hyperpolarization is applied in the last third phase of the ISI (Fig.8.D.), which is in agreement with the experimental results (Bennett and Wilson, 1998). However it was able to show prominent phase advance in the middle of the ISI cycle, which was not seen in the experiments (Bennett and Wilson, 1998). This is because due to the hyperpolarizing current injections the amplifying effect of the G_{kir} pulls the membrane potential down close to the potassium equilibrium, abruptly resetting the phase and introducing a prominent phase advance (Fig.8.B.E.). Therefore we conclude that the subthreshold mechanism analyzed in this study is not sufficient

to explain the experimental observations for the abilities of the IPSP-s to control the timing precision of the AchN-s.

In summary, our simulations indicate that in *regime I.* and *regime III.* the counteracting amplifying and dampening effects of the two conductances are acting in different ratios (Fig.3.B.). In *regime II.* (Fig.3.B.) the incoming synaptic events' amplification is time dependent, and is a function of when they occur during the ISI. Therefore we conclude that the amplification is conditional on the injected current parameter regime and on the timing of the synaptic events in the ISI. Thus it is likely to be a more elaborate process than earlier experimental results suggested (Wilson, 2005).

Effect of the dopaminergic modulation on the very slow frequency oscillation

We have implemented the dopaminergic influence on the $G_{Ca_v.1}$ (L-type) calcium conductance and found that the dopaminergic effect increases the amplitude and the maximum voltage value of the stable periodic solution of this very slow amplitude periodic solution (Fig.9.A.). On the other hand the frequency of the periodic solution is just slightly decreased as a function of the $\overline{g}_{Ca}$ (Fig.9.B.). This prediction is in agreement with the experimental finding showing D_1 receptor-mediated enhancement of the afterhyperpolarization (AHP) (Bennett and Wilson, 1998) and that dopamine induces a membrane depolarization on the AchN-s via activation of postsynaptic D_1-like receptors (Aosaki et al., 1998). It is important to note that D_2 receptor mediated effects on $G_{Ca_v.2.2}$ (N-type) and on Na^+ conductances are not responsible for this type of low frequency oscillation, thus the effects of those conductances are not analyzed here (Cabrera-Vera et al., 2004),(Yan et al., 1997),(Maurice et al., 2004),(Pisani et al., 2007).

Discussion

Intrastriatal release of dopamine and inhibition of interneuron activity is thought to be a critical link between behaviorally relevant events, such as reward, and alterations in striatal function. In this computational study we have investigated how the subthreshold autonomous oscillatory behavior of the AchN is influenced by dopaminergic modulation and how the synaptic voltage changes are sculptured by the subthreshold hyperpolarization activated conductances.

Implications of the results

As striatal dopamine level falls, striatal acetylcholine release increases, causing motor symptoms. This is mostly attributed to the loss of interneuronal regulation by inhibitory D_2 dopamine receptors (Ding et al., 2006). The attenuation of in-

terneuronal autoreceptor signaling might significantly contribute to the elevation of striatal acetylcholine release in Parkinson's disease (Ding et al., 2006). The chronic effects of dopaminergic receptors on the physiology and on the pathology of striatal neurons are relatively well studied and documented. By contrast the effects of acute dopamine depletion on striatal neurons remain poorly explored Fino et al. (2007). Recent experimental study revealed, that after acute dopamine depletion cholinergic cells displayed an increased excitability (Fino et al., 2007). Such acute and chronic membrane property changes indicate that striatal circuits should undergo major alteration on different time-scales. Therefore it is possible, that regulation of the striatal ACh system by dopamine receptor subtypes is differentially affected such that the D_2 -mediated inhibitory influence no longer predominates over the D_1 -mediated excitatory drive (DeBoer and Abercrombie, 1996). This would also imply that the opposing effects of the D_1 and D_2 receptors on the autonomous subthreshold oscillations (what we demonstrated in this study) are also acting on different timescales.

In agreement with the experimental findings, our results suggest that the duration of hyperpolarizing potentials in the spontaneous subthreshold oscillation is determined by the G_h's time constant, rather than the duration of the hyperpolarizing synaptic potentials (Wilson, 2005). We have found that with physiological conductance values the model is at the edge of the regime where it exhibits periodic oscillatory solution (Wilson, 2005). This result suggests a high susceptibility of the dynamics to dopaminergic modulation, thus the dopamine is able to switch the subthreshold dynamics easily between periodic oscillatory and fixed point solutions.

Experimental study showed that the IPSPs are only influencing the overall firing rate of the AchN-s (Bennett and Wilson, 1998), but our simulations predict that they are able to contribute to the spike timing as well. In the simulations the amplification of the hyperpolarizing events are also dependent on the phase of the oscillation (Fig.8.B.). The closer the synaptic event arrives to the deactivation of the G_h in the middle of the cycle, the more likely that the hyperpolarizing effect of the G_{kir} dominates, and thus we observe a phase advance and at the same time the synaptic event is amplified (Fig.8.F.). The latter agrees with the experimental observations which shows that the amplitude of the IPSP-s is strongly dependent on when the IPSP occurred during the ISI (Bennett and Wilson, 1998). On the other hand in the simulations the amplitude of the evoked potentials is a non-monotonic function of the phase at which the current arrived (Fig.8.F.). This is again due to the G_h activation in the hyperpolarized state of the autonomous oscillation, which has counteracting effect with the hyperpolarizing current steps, therefore in the last part of the cycle the amplitude decreased (Fig.8.F.). One possible explanation for the difference between the experimental findings and our simulation results is that the AchNs might receive the GABA-ergic innervation on a different neuronal compartment than the excitatory ones, which are expressing the hyperpolarization activated conductances (Harris et al., 2002).

Limitations of the model

It is important to note that there is evidence about the spatial segregation of the G_{kir} and G_h conductances in striato-pallidal medium spiny neurons (Shen et al., 2007). We have modelled the cholinergic interneurons as a point neuron (without spatial extension), in the very same way as previous studies have done (Wilson, 2005), (Wilson and Goldberg, 2006), since we have found no experimental evidence about the spatial segregation of these conductances. In several cases it might well be, that using the simplest model which still explains a certain phenomena leads to deeper understanding, making the mathematical analysis of the model possible.

In the present modelling study we did not implement the spike generating mechanism of the AchN-s. Although the dopamine induced reduction in striatal cholinergic interneuron activity is also influenced by the modulated Na^+ currents (Maurice et al., 2004), we restricted our analysis on the dopaminergic effect of G_{kir} and G_h and on the L-type calcium- and calcium current dependent potassium conductances. These conductances are responsible for the medium and low frequency autonomous subthreshold oscillations. Further studies should explore the modulatory effects of the D_1 and D_2 receptors on the AchN's dynamics incorporating the suprathreshold spike generating conductances as well.

Possible further directions

Immune-histological studies have found that anti-$Kir2.4$ antibodies react with many neurons in the striatum, but they most intensely stain the AchN-s (Pruss et al., 2003). The compartmental organization of the striatum is also reflected in the different Kir subunit containing potassium channels (i.e. $Kir2.4$ versus $Kir2.3$). Since the output of the patch and matrix compartments are different (primarily influence on the motor circuits versus on the limbic system), targeting and disconnecting $Kir2.3$ or $Kir2.4$ channel activation may participate in an improved therapy, significantly and selectively reducing psychotic and motor side-effects (Pruss et al., 2003). Further modeling studies should examine the dynamic consequences of the differences between $Kir2.3$ and $Kir2.4$ subunit containing conductances. Similarly, at least two G_h channel subunits are present in the AchN-s (Santora et al., 2000). The combination of the two is critical for determining the voltage sensitivity and the time constant of the I_h, thus for the excitability of the AchN. To determine the consequences of this effect also requires further experimental and modelling investigation.

A recent *in vitro* experimental study demonstrated that increased occurrence of spontaneous bicuculline-sensitive depolarizing postsynaptic potentials (sDPSP) was recorded from those AchN-s, which were obtained from trained rats (Bonsi et al., 2003). The frequency of the $GABA_A$-mediated postsynaptic potentials (sDPSP) was increased in comparison to not-conditioned rats. These results suggested that after learning a rewarded sensorimotor paradigm an increased GABA influence de-

velops on cholinergic interneurons. This intrastriatal mechanism might be partially involved in the phasic suppression of discharge of TANs at the presentation of reward-related sensory stimuli (Bonsi et al., 2003). Our modelling study predicts that besides the possibly increased GABA influence, the dopaminergic modulation is also able to contribute to this experimental observation. Thus the sDPSP increase could be attributable to the dopaminergic modification of the two hyperpolarization activated conductances.

The *in vivo* AchN pause might provide a dynamic window for the dopamine signal in the striatum Cragg (2006). The pause response has the potential to amplify DA signals associated with DA bursts (reward related stimuli evoked) (Cragg, 2006). This is probably how the TANs participate in DA-dependent reward related signalling and reinforcement learning (Cragg, 2006). Further investigation is required into how the ongoing nicotinic activity enhances the dopamine release, providing a negative feed-back in the system (Zhou et al., 2002). This latter is particularly important, because it seems that the pause in the AchN release alters action potential dependent dopamine release (Zhou et al., 2002).

1 Appendix

Simplifying notations in the model of the medium frequency oscillation:

V_m	x
h	y
g_h	**a**
g_{kir}	**b**
E_h	c
$V_{(1/2)h}$	f
$V_{(s)h}$	p
τ_h	k
E_{kir}	d
$V_{(1/2)kir}$	m
$V_{(s)kir}$	t
g_{leak}	w
E_{leak}	h
I_{inj}	j

The *parametric representation method* (PRM) was applied to construct bifurcation diagrams analytically (Simon et al., 2001), (Simon et al., 1999). We were able to use the PRM, because the parameter a and b (those which are modulated by dopamine) linearly influence the variables (Simon et al., 2001), (Simon et al., 1999). The 2-dimensional system (for the medium frequency oscillation) with simplified notation is the following (from eqns 1. and 4.):

$$\frac{dx}{dt} = -(ay(x-c)) - \frac{b(x-d)}{1+exp(\frac{x-m}{t})} - w(x-h) + j \quad (16) \qquad \frac{dy}{dt} = \frac{1}{k(1+exp(\frac{x-f}{p}))} - \frac{y}{k} \quad (17)$$

The Jacobian matrix of the above two-dimensional system is the following:

$$J = \begin{pmatrix} -ay - \frac{b(1+exp(\frac{x-m}{t}))-b(x-d)exp(\frac{x-m}{t})\frac{1}{t}}{(1+exp(\frac{x-m}{t}))^2} - w & -a(x-c) \\ \\ \frac{-\exp(\frac{x-f}{p})}{k(1+exp(\frac{x-f}{p}))^2 p} & -\frac{1}{k} \end{pmatrix} \quad (18)$$

In a 2D case the Hopf bifurcation diagram can be obtained from the following conditions: the *trace* of the Jacobian matrix J should be zero ($Tr(J) = 0$), and $det(J)$ should be bigger than zero (Simon et al., 2001), (Simon et al., 1999). From the zero *trace* condition we write:

$$0 = -ay - \frac{b(1 + exp(\frac{x-m}{t})) - b(x-d)exp(\frac{x-m}{t})\frac{1}{t}}{(1 + exp(\frac{x-m}{t}))^2} - w - \frac{1}{k}. \tag{19}$$

The steady state original equation from eqn. 16. is the following:

$$0 = -(ay(x-c)) - \frac{b(x-d)}{1 + exp(\frac{x-m}{t})} - w(x-h) + j. \tag{20}$$

From egn. 17.:

$$y = \frac{1}{1 + exp(\frac{x-f}{p})}, \tag{21}$$

hence the 2D system can be reduced to a single algebraic equation:

$$0 = \frac{-a(x-c)}{1 + exp(\frac{x-f}{p})} - \frac{b(x-d)}{1 + exp(\frac{x-m}{t})} - w(x-h) + j. \tag{22}$$

From the zero *trace* condition we obtain:

$$0 = \frac{-a}{1 + exp(\frac{x-f}{p})} - \frac{b(1 + exp(\frac{x-m}{t})) - b(x-d)exp(\frac{x-m}{t})\frac{1}{t}}{(1 + exp(\frac{x-m}{t}))^2} - w - \frac{1}{k}. \tag{23}$$

Simplifying the notations (in equations 22,23) we obtain:

$$0 = aF_1(x) + bF_2(x) + F_3(x) \quad (24) \qquad 0 = aG_1(x) + bG_2(x) + G_3(x) \quad (25)$$

where:

$$F_1 = \frac{c-x}{1 + exp(x_1)}, \quad (26) \quad F_2 = \frac{d-x}{1 + exp(x_2)}, \quad (27) \quad F_3 = j + w(h-x), \quad (28)$$

$$G_1 = \frac{-1}{1 + exp(x_1)}, \quad (29) \qquad G_2 = -\frac{1 + exp(x_2) + (d-x)exp(x_2)}{(1 + exp(x_2))^2}, \quad (30)$$

$$G_3 = -w - \frac{1}{k}, \quad (31) \qquad x_1 = \frac{x-f}{p}, \quad (32) \qquad x_2 = \frac{x-m}{t}. \quad (33)$$

From the above equations (24., 25.) a and b can be expressed as a function of x. :

$$a(x) = \frac{G_3F_2 - F_3G_2}{F_1G_2 - G_1F_2}, \quad (34) \qquad b(x) = \frac{G_1F_3 - F_1G_3}{F_1G_2 - G_1F_2}. \quad (35)$$

Other necessary condition for the Hopf bifurcation is that the $det(J)$ should be bigger than zero (Simon et al., 2001), (Simon et al., 1999). We have checked this condition as well in the relevant parameter regimes. We were able to reproduce with the PRM the numerically obtained 2-dimensional bifurcation diagram (Fig.7.A).

Acknowledgments

We thank to Peter Simon and Ferenc Mátyás for useful discussions, John Tepper, Ping Deng for sending us relevant literature on this field and Suresh Krishna for carefully reading the manuscript and correcting the english. KSz was supported by the Eötvös Fellowship, and part of this study was done at KTH, Stockholm. This work was further supported by the EU Sixth Framework programme (grant no.: IST-4-027819-IP, ICEA).

Figure legends

Figure 1.
Voltage traces of the medium frequency subthreshold autonomous oscillation at two different parameter regimes. The injected current was set to zero in these simulations. **(Figure A.)** We changed the $\overline{g_{kir}}$, while kept the $\overline{g_h} = 2\,\mathrm{mS/cm^2}$ constant.**(Figure B.)** We changed the $\overline{g_h}$ parameter, while keeping the $\overline{g_{kir}} = 2.75\,\mathrm{mS/cm^2}$ constant.

Figure 2.
Bifurcation analysis of the point neuron model producing medium frequency oscillation **(Figure A-C.)**. Dashed and solid lines are stable periodic solutions and stable fixed points (of the membrane potential variable solution) respectively, and stars and empty dots denote unstable fixed points and unstable periodic solutions.

(Figure 2.A.) Bifurcation analysis, where we changed the $\overline{g_h}$ conductance ($\overline{g_{kir}} = 2.75\,\mathrm{mS/cm^2}$). Voltage dependent τ_h was used in these simulations. Two vertical dashed lines represent the parameter values which were used in Fig.2.C.D. while determining dynamic regimes. The effect of dopamine (D_2) is noted with "←". The effect of dopamine (D_1) is noted with "→". The injected current was set to zero in all of these simulations.

(Figure 2.B.) Frequency information of the stable periodic solutions in the same study. Voltage dependent τ_h was used in these simulations. Two vertical dashed lines represent the parameter values which were used in Fig.2.C.D. while determining dynamic regimes. The effect of dopamine (D_2) is noted with "←". The effect of dopamine (D_1) is noted with "→".

(Figure 2.C.) Bifurcation analysis, where we changed the injected current parameter. Dashed and solid lines are stable periodic solutions and stable fixed points (of the membrane potential variable solution) respectively, and stars and empty dots denote unstable fixed points and unstable periodic solutions. Voltage dependent τ_h was used in all of these simulations. Two simulation results are shown with two different $\overline{g_h}$ values. The parameter values, which were noted with two vertical dashed lines on Fig. 2.A.B were used.

(Figure 2.D.) Frequency information of the periodic solutions in the same study. The parameter values, which were noted with two vertical dashed lines on Fig. 2.A.B were used.

Figure 3.
(Figure 3.A.) Boltzmann-functions of the two hyperpolarization activated conductances. Both half activation values are at -90 mV. The equilibrium potentials of the two conductances are shown as well.

(Figure 3.B.) Bifurcation analysis of the medium frequency oscillation model with two ($\overline{g_{kir}} = 2.75\,\mathrm{mS/cm^2}$, $1\,\mathrm{mS/cm^2}$) values. With the lower $\overline{g_{kir}}$ value there is no periodic solution. We divided the parameter regime into 3 different regions, depending on whether the model with $\overline{g_{kir}} = 2.75\,\mathrm{mS/cm^2}$ exhibit periodic solution or stable fixed point. In regimes I. and III. we compared the steepness of the steady state I/V relations, such that we shifted the I/V curves to each other, and followed how does the steepness change to hyperpolarizing direction.

Figure 4.
(Figure 4.A.) Bifurcation analysis, where we changed the half activation voltage value of the G_h ($\overline{g_{kir}} = 2.75\,\mathrm{mS/cm^2}$). Voltage dependent τ_h was used in all of these simulations. We have noted with "←" the dopamine induced shift in the half activation voltage value of the G_h.

(Figure 4.B.) Frequency information of the stable periodic solutions in the same study. We have noted with "←" the dopamine induced shift in the half activation voltage value of the G_h.

(Figure 4.C.) Bifurcation analysis, where we changed the injected current, two simulation results are shown at two different half activation voltage values. Voltage dependent τ_h was used in all of these simulations.

(Figure 4.D.) Frequency information of the periodic solutions in the same study.

Figure 5.

(Figure 5.) Bifurcation analysis, where we changed the time constant of the $\overline{g_h}$ conductance. The two hyperpolarization activated conductance values were set to $\overline{g_{kir}} = 2.75\text{mS/cm}^2$ and $\overline{g_h} = 2\,\text{mS/cm}^2$. On **Figure 5.A.** results with two parameter values were examined ($\tau_h = 250\,\text{ms}$ and $\tau_h = 350\,\text{ms}$). In this simulation set voltage independent τ_h-s were used.

(Figure 5.B.) Frequency information of the periodic solutions in the same study.

(Figure 5.C.) Bifurcation analysis, where we changed the time constant of the G_h. The conductances were set to $\overline{g_{kir}} = 2.75\,\text{mS/cm}^2$ and $\overline{g_h} = 2\,\text{mS/cm}^2$. The injected current value were $I_{inj} = 0\,\mu\text{A/cm}^2$, $I_{inj} = -2\,\mu\text{A/cm}^2$, $I_{inj} = -4\,\mu\text{A/cm}^2$.

(Figure 5.D.) Frequency information of the periodic solutions in the same study.

Figure 6.
Bifurcation analysis of the point neuron model producing medium frequency oscillation **(Figure A-D.)**. The bifurcation parameter is the maximal conductance value of $\overline{g_{kir}}$. Dashed and solid lines are stable periodic solutions and stable fixed points (of the membrane potential variable solution) respectively, and stars and empty dots denote unstable fixed points and unstable periodic solutions. Voltage dependent τ_h was used in these simulations.

(Figure 6.A.) Bifurcation analysis, where the $\overline{g_{kir}}$ was altered ($\overline{g_h} = 2\,\text{mS/cm}^2$). The vertical dashed line represents the parameter value which was used in Fig.6 C.-D. while determining dynamic regimes. The effect of dopamine (D_1) is noted with "←", while the increase of the $\overline{g_{kir}}$ parameter value was noted with "→". The injected current was set to zero in these simulations.

(Figure 6.B.) Frequency information of the periodic solutions in the same study. The vertical dashed line represents the parameter value which was used in Fig.6.C.-D. while determining dynamic regimes. The effect of dopamine (D_1) is noted with "←", while the increase of $\overline{g_{kir}}$ elevation was noted with "→".

Figure 6.C-D. Bifurcation analysis, where we changed the injected current parameter. Dashed and solid lines are stable periodic solutions and stable fixed points (of the membrane potential variable solution) respectively, and stars and empty dots denote unstable fixed points and unstable periodic solutions. Voltage dependent τ_h was used in all of these simulations.

(Figure 6.C.) Bifurcation analysis, where we changed the injected current at two different $\overline{g_{kir}}$ conductance values. The parameter value, which was noted with the right vertical dashed line on Fig. 6.A.B. was used ($\overline{g_{kir}} = 6\,\text{mS/cm}^2$, $\overline{g_{kir}} = 2.75\,\text{mS/cm}^2$).

(Figure 6.D.) Frequency information of the periodic solutions in the same study. The parameter value, which was noted with the right vertical dashed line on Fig.6.A.B. was used ($\overline{g_{kir}} = 6\,\text{mS/cm}^2$, $\overline{g_{kir}} = 2.75\,\text{mS/cm}^2$).

Figure 7.

Quantitative analysis on the change of special points in two dimensional parameter space in the medium frequency oscillation. On **Figure 7.A.** we examined the shift of the special points in the $\overline{g_h}$-$\overline{g_{kir}}$ maximal conductances two dimensional parameter space. The dynamic range change of the point neuron can be followed as the change of the area between the two Hopf bifurcation curves. The injected current was set to zero in all of these simulations. Vertical and horizontal dashed lines represent the parameter values found in the literature without dopaminergic modulation.The dopaminergic effect was considered on different receptors according to the experimental literature (Table 1.).

On **Figure 7.B.** we presented results in the same two dimensional space, where we demonstrated the frequency values of the subthreshold oscillation frequencies.

On **Figure 7.C.** in the same two dimensional space we demonstrated the maximal membrane potential values of the subthreshold oscillations (the peak values of the periodic stable solutions).

(Figure 8.)
In *regime II.* of Fig.3.B the phase response curves and the amplification of the depolarizing (Figure 8.A.) and hyperpolarizing (Figure 8.B.) events were examined. Hyperpolarizing short current steps were applied, ($\pm 5\,\frac{\mu A}{cm^2}$ for 50 msec). The amplitude of membrane potential was calculated such that from the peak value of the evoked membrane potential the membrane potential value was subtracted, which is reached at the same time but without additional current steps applications (black curves on Figure 8.A.B.). EP refers to the *evoked membrane potential*. One period was considered between two consecutive most depolarized states (**Figure 8.A.B.**). The amplitude of the EPs are notified by dashed lines on Figure 8.A.B. The cycle containing the perturbation has the length of period T_1 and T_0 is the length without the perturbation. We defined the phase resetting as:

$$\Delta\Phi = \frac{T_1 - T_0}{T_0} \tag{36}$$

The phase response curves for depolarizing (**Figure 8.C.**) and hyperpolarizing (**Figure 8.E.**) current injections were obtained. (**Figure 8.D.**) shows EPSP amplitudes, as a function of the time within one subthreshold oscillation cycle.(**Figure 8.F.**) shows IPSP amplitudes, as a function of the time within one subthreshold oscillation cycle.

(Figure 9.A.B.) Bifurcation analysis, the bifurcation parameter was the $\overline{g}_{Ca}$. Dashed and solid lines are stable periodic solutions and stable fixed points (of the membrane potential variable solution) respectively, and stars denote unstable fixed point solutions. Fig.**A.** shows the stable fixed point and periodic solutions of the membrane potential, and Fig.**B.** has the frequency information of the periodic solutions in the same study. The injected current was set to zero in all of these simulations. Vertical dashed lines represent the parameter values which reproduced the subthreshold very low frequency oscillation. The effect of dopamine (D_1) is noted with "$\rightarrow$".

Tables

Table 1.

It is accepted that activation of different dopamine receptor subtypes elicits distinct effects on cholinergic interneurons (Aosaki et al., 1998), (Yan et al., 1997).

conductance	Dopaminerg effect through D_1	Dopaminerg effect through D_2
G_h $V_{(1/2)}$		⟵ (Deng et al., 2007)
G_h	↑ (Aosaki et al., 1998)	↓ (Deng et al., 2007)
G_{kir}	↓ (Aosaki et al., 1998)	
G_{kir}	↑ Dopamine maintains M_4 receptor activated KIR conductance (Ding et al., 2006),(Calabresi et al., 1998),(Pisani et al., 2007)	
$G_{Ca^{2+}}$ (N-type)		↓ (Cabrera-Vera et al., 2004) (Yan et al., 1997), (Pisani et al., 2007),
$G_{Ca^{2+}}$ (L-type)	↑ (Surmeier et al., 1995) (Bennett and Wilson, 1998)	
G_{Na^+}		↓ (Maurice et al., 2004)

Table 1. summarizes the experimental literature about the dopaminergic modulatory effects on the AchN's conductances through D_1 and D_2 receptors. "↑" refers to increase, "↓" to decrease, and we noted with "⟵" that the half activation voltage is moving to more hyperpolarized value.

Table 2.

E_h	-40 mV
E_l	-60 mV
E_K	-90 mV
$V_{(1/2)h}$	-90 mV
$V_{(1/2)kir}$	-90 mV
$V_{(s)h}$	6 mV
$V_{(s)kir}$	6 mV
$\overline{g_{kir}}$	$2.75\,\mathrm{mS/cm^2}$
$\overline{g_l}$	$0.08\,\mathrm{mS/cm^2}$
$\overline{g_h}$	$2\,\mathrm{mS/cm^2}$
C	$1\,\mu\mathrm{F/cm^2}$

Table 3.

d	$10\mu m$
τ_{Ca}	$0.1\frac{s}{\mu m}$
buf	0.1
$\overline{g_{sAHP}}$	$0.3\frac{mS}{cm^2}$
$\overline{g_{Ca}}$	$0.015\frac{mS}{cm^2}$
$\overline{g_{Kv}}$	$0.04\frac{mS}{cm^2}$
$\overline{g_{leak}}$	$0.001\frac{mS}{cm^2}$
V_{Ca}	$100\,mV$
V_K	$-90\,mV$
V_{leak}	$-50\,mV$
$V_{(1/2)Ca}$	$-20\,mV$
$V_{(s)Ca}$	$6\,mV$
$V_{(1/2)Kv}$	$-14\,mV$
$V_{(s)Kv}$	$6\,mV$
α	$0.005\frac{nM}{s}$
β	$0.25\frac{nM}{s}$

References

Alcantara, A., Chen, V., Herring, B., Mendenhall, J., Berlanga, M., 2003. Localization of dopamine D_2 receptors on cholinergic interneurons of the dorsal striatum and nucleus accumbens of the rat. Brain Research 986, 22–29.

Aosaki, T., Kiuchi, K., Kawaguchi, Y., 1998. Dopamine D_1-like receptor activation excites rat striatal large aspiny neurons in vitro. J. of Neurosci. 18(14), 5180–5190.

Bennett, B., Wilson, J., 1998. Synaptic regulation of action potential timing in neostriatal cholinergic interneurons. J. of Neurosci. 18(20), 8539–8549.

Bonsi, P., Florio, T., Capozzo, A., Pisani, A., Calabresi, P. Siracusano, A., Scarnati, E., 2003. Behavioural learning-induced increase in spontaneous GABAA-dependent synaptic activity in rat striatal cholinergic interneurons. Eur. J. Neurosci. 17(1), 174–8.

Cabrera-Vera, T., Hernandez, S., Earls, L., Medkova, M., Sundgren-Andersson, A., Surmeier, J., Hamm, E., 2004. RGS9-2 modulates D2 dopamine receptor-

mediated Ca2+ channel inhibition in rat striatal cholinergic interneurons. PNAS 101(46), 16339–16344.

Calabresi, P., Centonze, D., Pisani, A., Sancesario, G., North, R., Bernardi, G., 1998. Muscarinic IPSPs in rat striatal cholinergic interneurones. J. Physiol. 510, 421–7.

Consolo, S., Girotti, P., Russi, G., Di Chiara, G., 1992. Endogenous dopamine facilitates striatal in vivo acetylcholine release by acting on d1 receptors localized in the striatum. J Neurochem. 59(4), 1555–7.

Cragg, S., 2006. Meaningful silences: how dopamine listens to the ACh pause. TRENDS in Neuroscience 29., 125–131.

Damsma, G., Tham, C., Robertson, G., Fibiger, H., 1990. Dopamine D1 receptor stimulation increases striatal acetylcholine release in the rat. Eur. J. Pharmacology 186(2-3), 335–8.

DeBoer, P., Abercrombie, E., 1996. Physiological release of striatal acetylcholine in vivo: modulation by d1 and d2 dopamine receptor subtypes. J. Pharmacol. Exp. Ther. 277(2), 775–83.

DeBoer, P., Westerink, B., 1994. GABA-ergic modulation of striatal cholinergic interneurons: An in vivo microdialysis study. J. of Neurochemistry 62(1), 70–5.

Deng, P., Zhang, Y., Xu, Z., 2007. Involvement of I(h) in dopamine modulation of tonic firing in striatal cholinergic interneurons. J. of Neurosci. 27(12), 3148–56.

Ding, J., Guzman, J., Tkatch, T., Chen, S., Goldberg, J., Ebert, P., Levitt, P., Wilson, C., Hamm, H., Surmeier, D., 2006. RGS4-dependent attenuation of M4 autoreceptor function in striatal cholinergic interneurons following dopamine depletion. Nature Neuroscience 9(6), 832–42.

Ding, Y., Logan, J., Bermel, R., Garza, V., Rice, O., Fowler, J., Volkow, N., 2000. Dopamine receptor-mediated regulation of striatal cholinergic activity: positron emission tomography studies with norchloro[18f]fluoroepibatidine. J. of Neurochemistry 75(4), 1514–1521.

Exley, R., Cragg, S., 2007. Presynaptic nicotinic receptors: a dynamic and diverse cholinergic filter of striatal dopamine neurotransmission. Br. J. Pharmacol. 7, 1–15.

Fino, E., Glowinskib, J., Venance, L., 2007. Effects of acute dopamine depletion on the electrophysiological properties of striatal neurons. Neuroscience Research 58(3), 305–16.

Harris, K., Henze, D., Hirase, H., Leinekugel, X., Dragoi, G., Czurk, A., Buzski, G., 2002. Spike train dynamics predicts theta-related phase precession in hippocampal pyramidal cells. Nature 417(6890), 738–41.

Huguenard, J., McCormick, D., 1992. Simulation of the currents involved in rhythmic oscillations in thalamic relay neurons. J. of Neurophysiol. 68, 1373–1383.

Izhikevich, E., 2002. Dynamical Systems in Neuroscience: The Geometry of Excitability and Bursting. The MIT Press, Cambridge, MA.

Mao, B., MacLeish, P., Victor, J., 2003. Role of hyperpolarization-activated currents for the intrinsic dynamics of isolated retinal neurons. Biophys. J. 84(4), 2756–67.

Maurice, N., Mercer, J., Chan, C., Hernandez-Lopez, S., Held, J., Tkatch, T., Surmeier, D., 2004. D_2 dopamine receptor-mediated modulation of voltage-dependent Na^+ channels reduces autonomous activity in striatal cholinergic interneurons. J. of Neurosci. 24(46), 10289–301.

Peck, J., E. Gaier, E. Stevens, S. R., Harris-Warrick, R. M., 2006. Amine modulation of I_h in a small neural network. J. of Neurophysiol. 96(6), 2931–40.

Pisani, A., Bernardi, G., Ding, J., Surmeier, D., 2007. Re-emergence of striatal cholinergic interneurons in movement disorders. TRENDS in Neurosciences 30(10), 545–553.

Pisani, A., Bonsi, P., Centonze, D., Calabresi, P., Bernardi, G., 2000. Activation of D_2-like dopamine receptors reduces synaptic inputs to striatal cholinergic interneurons. J. of Neurosci. 20(7), RC69.

Pruss, H., Wenzel, M., Eulitz, D., Thomzig, A., Karschin, A., Veh, R., 2003. Kir2 potassium channels in rat striatum are strategically localized to control basal ganglia function. Mol. Brain. Res. 110(2), 203–19.

Ravel, S., Sardo, P., Legallet, E., Apicella, P., 2006. Influence of spatial information on responses of tonically active neurons in the monkey striatum. J. of Neurophysiol. 95., 2975–2986.

Santora, B., Chen, S., Luthi, A., Pavlidis, P., Shumyatsky, G., Tibbs, G., Siegelbaum, S., 2000. Molecular and functional heterogeneity of hyperpolarization-activated pacemaker channels in the mouse CNS. J. of Neurosci. 20, 5264–5275.

Shen, W., Tian, X., Day, M., Ulrich, S., Tkatch, T., Nathanson, N., Surmeier, D., 2007. Cholinergic modulation of Kir2 channels selectively elevates dendritic excitability in striatopallidal neurons. Nature Neurosci. 10(11), 1458–66.

Simon, P., Farkas, H., Wittman, M., 1999. Constructing global bifurcation diagrams by the parametric representation method. J. Comp. Appl. Math. 108, 157–176.

Simon, P., Hild, E., Farkas, H., 2001. Relationships between the discriminant curve and other bifurcation diagrams. J. Mathematical Chemistry. 29(4), 245–265.

Surmeier, D., Bargas, J., Hemmings, H., Nairn, A., Greengard, P., 1995. Modulation of calcium currents by a D1 dopaminergic protein kinase/phosphatase cascade in rat neostriatal neurons. Neuron 14, 385–397.

Szalisznyó, K., 2006. Role of hyperpolarization-activated conductances in the lateral superior olive: a modeling study. J. of Computational Neurosci. 20(2), 137–52.

Watanabe, K., Kimura, M., 1998. Dopamine receptor-mediated mechanisms involved in the expression of learned activity of primate striatal neurons. J. of Neurophysiol. 79, 2568–2580.

Wessel, R., Koch, C., Gabbiani, F., 1996. Coding of time-varying electric field amplitude modulations in a wave-type electric fish. J. of Neurophysiol. 75(6), 2280–93.

Wilson, C., 2005. The mechanism of intrinsic amplification of hyperpolarizations and spontaneous bursting in striatal cholinergic interneurons. Neuron 45(4), 575–85.

Wilson, C., Chang, H., Kitai, S., 1998. Firing patterns and synaptic potentials of identified giant aspiny interneurons in the rat neostriatum. J. of Neurosci. 10, 508–519.

Wilson, C., Goldberg, J., 2006. Origin of the slow afterhyperpolarization and slow rhythmic bursting in striatal cholinergic interneurons. J. of Neurophysiol. 95(1), 196–204.

Yan, Z., Song, W., Surmeier, J., 1997. D2 dopamine receptors reduce N-type Ca^{2+} currents in rat neostriatal cholinergic interneurons through a membrane-delimited, protein-kinase-c-insensitive pathway. J. of Neurophysiol. 77(2), 1003–15.

Yan, Z., Surmeier, J., 1996. Muscarinic (M2/M4) receptors reduce N- and P-

type Ca2+ currents in rat neostriatal cholinergic interneurons through a fast, membrane-delimited, G-protein pathway. J. of Neurosci. 16(8), 2592–604.

Zhou, F., Wilson, C., Dani, J., 2002. Cholinergic interneuron characteristics and nicotinic properties in the striatum. J. of Neurobiol. 53(4), 590–605.

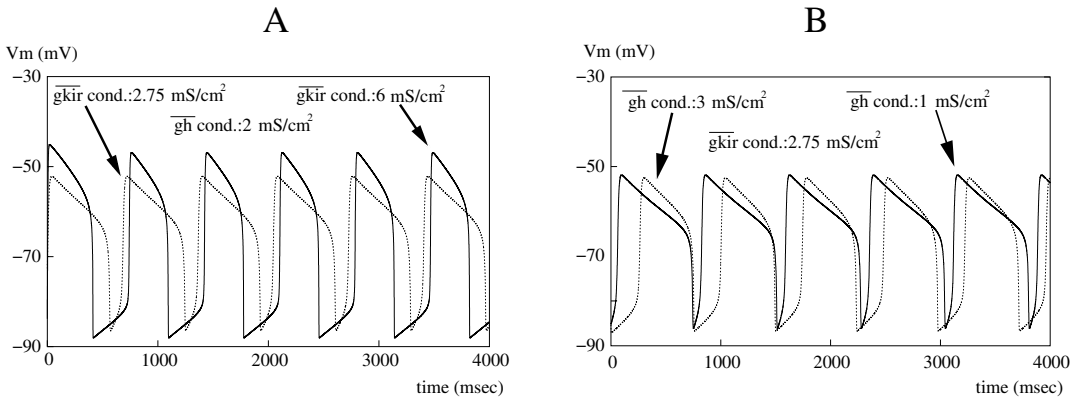

Fig. 1.

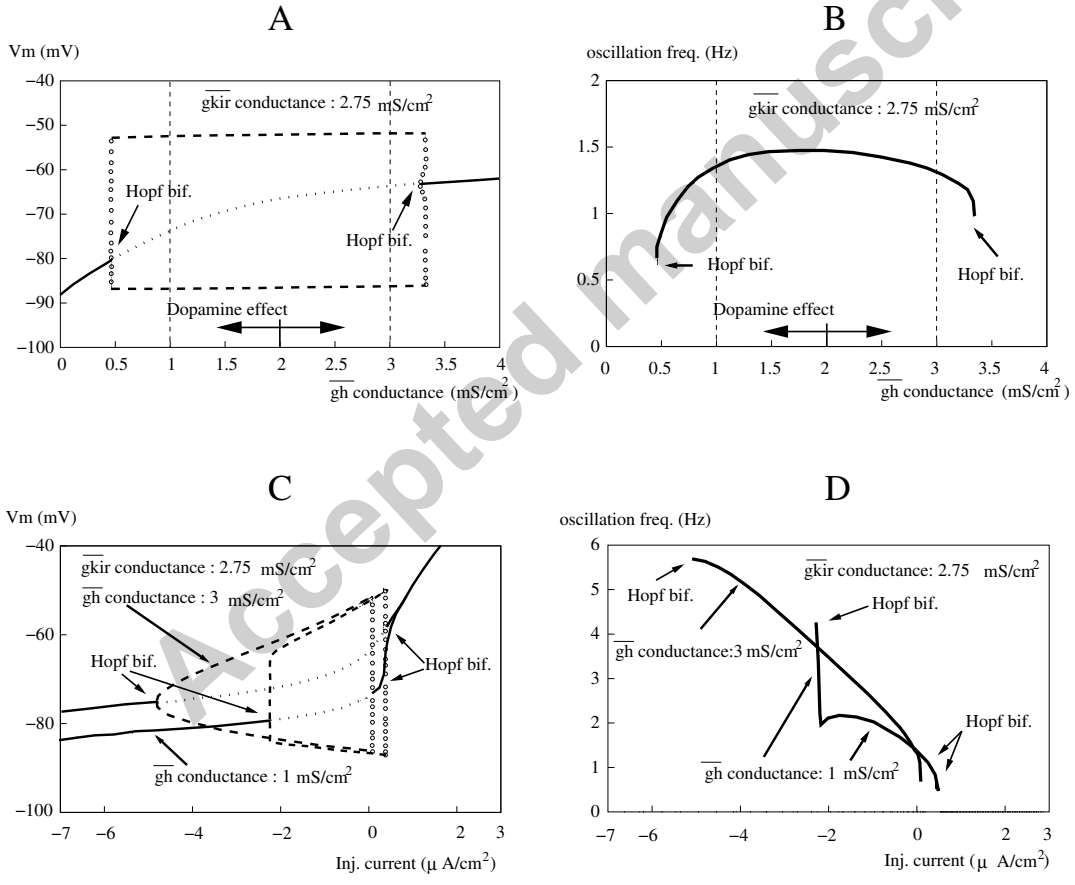

Fig. 2.

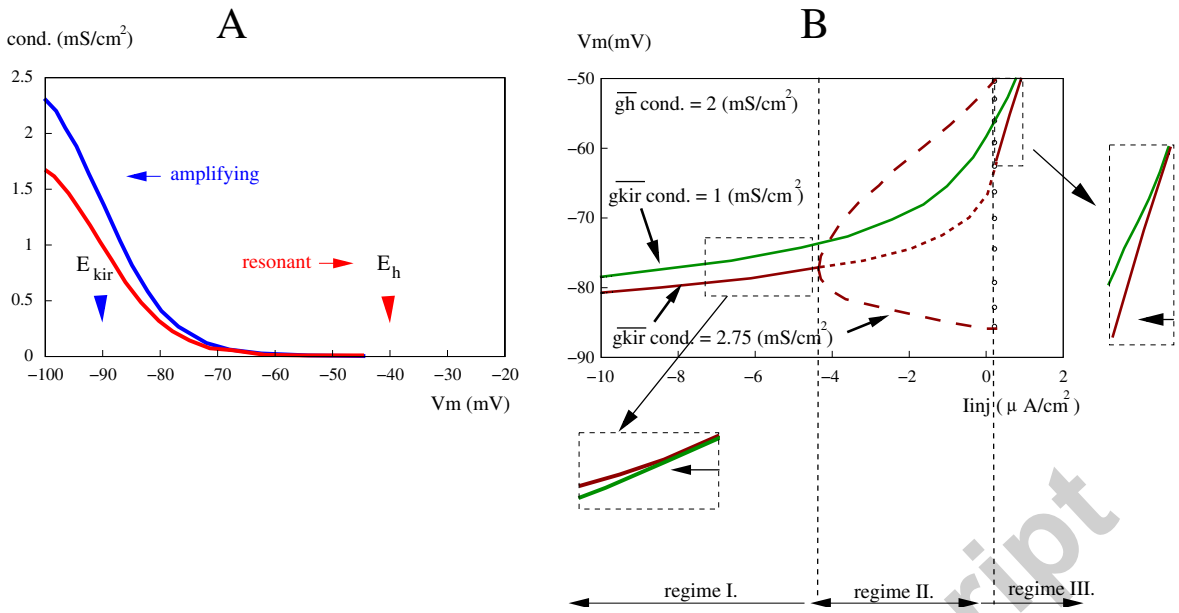

Fig. 3.

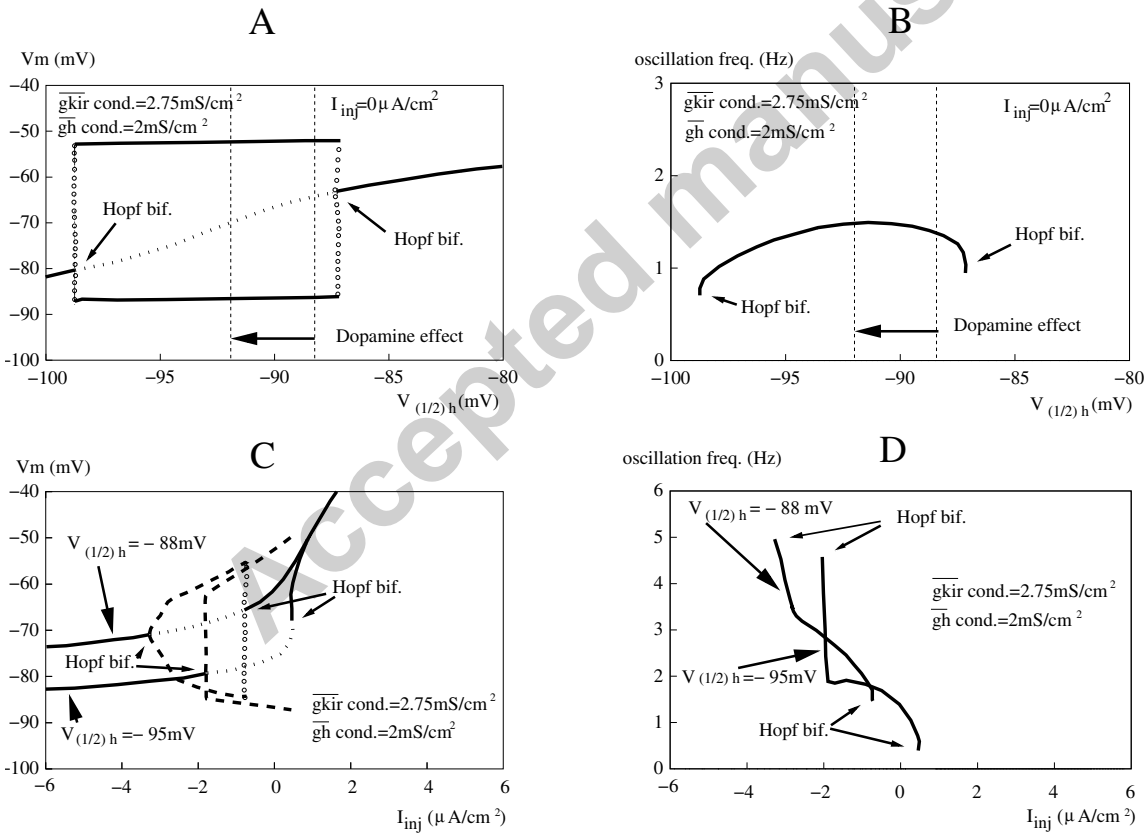

Fig. 4.

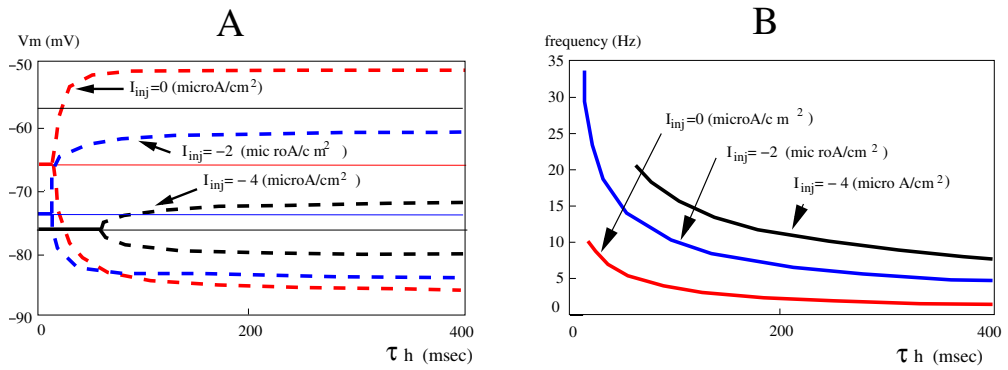

Fig. 5.

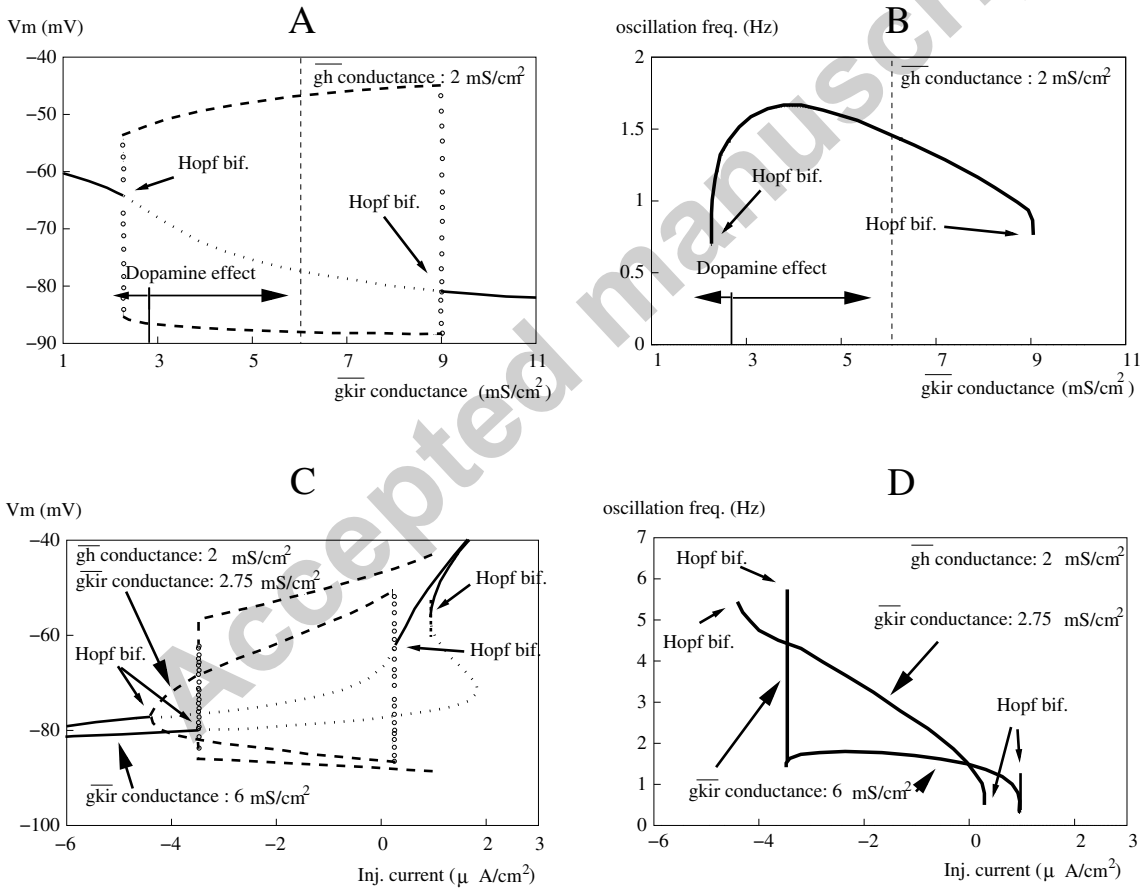

Fig. 6.

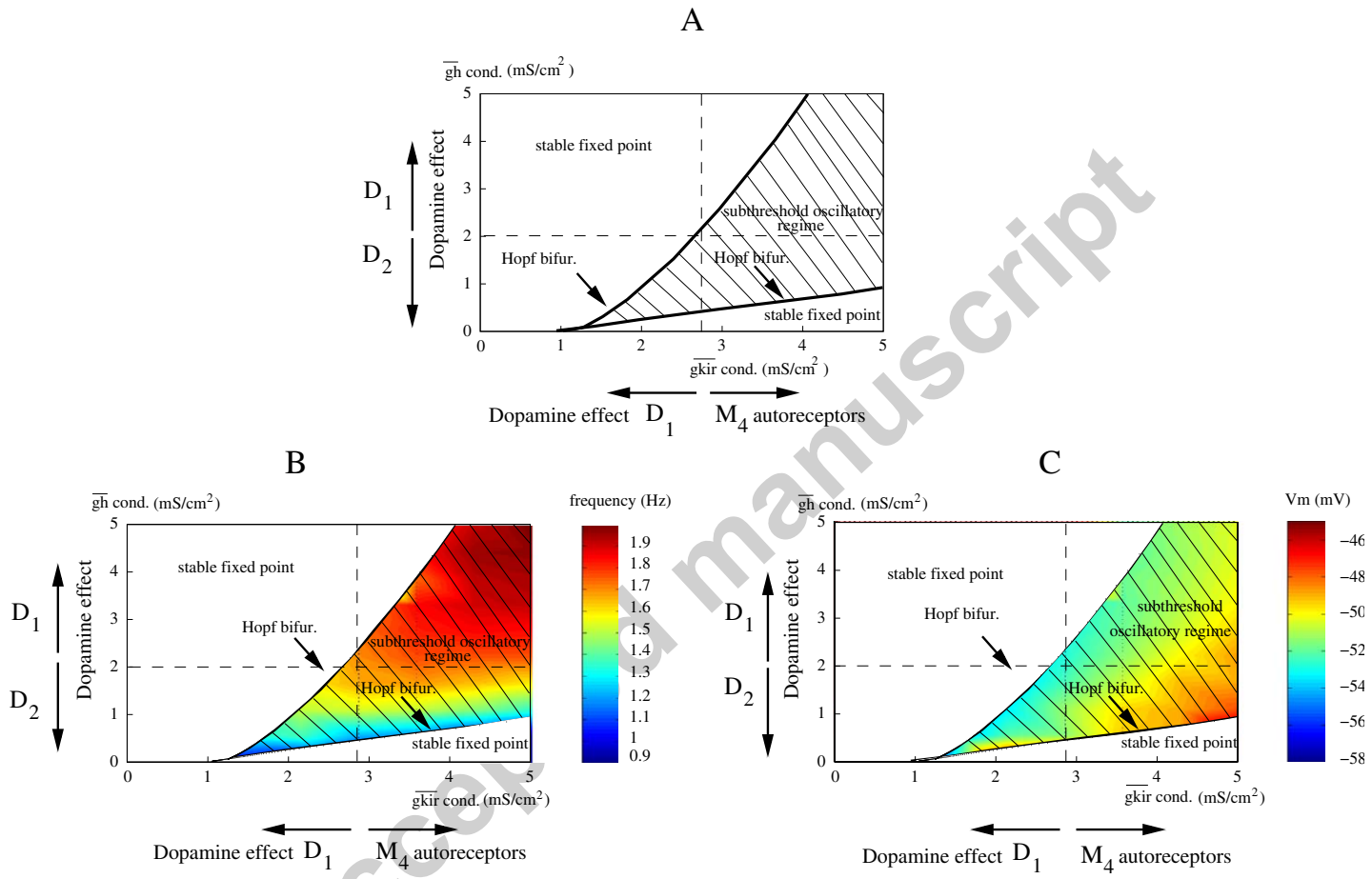

Fig. 7.

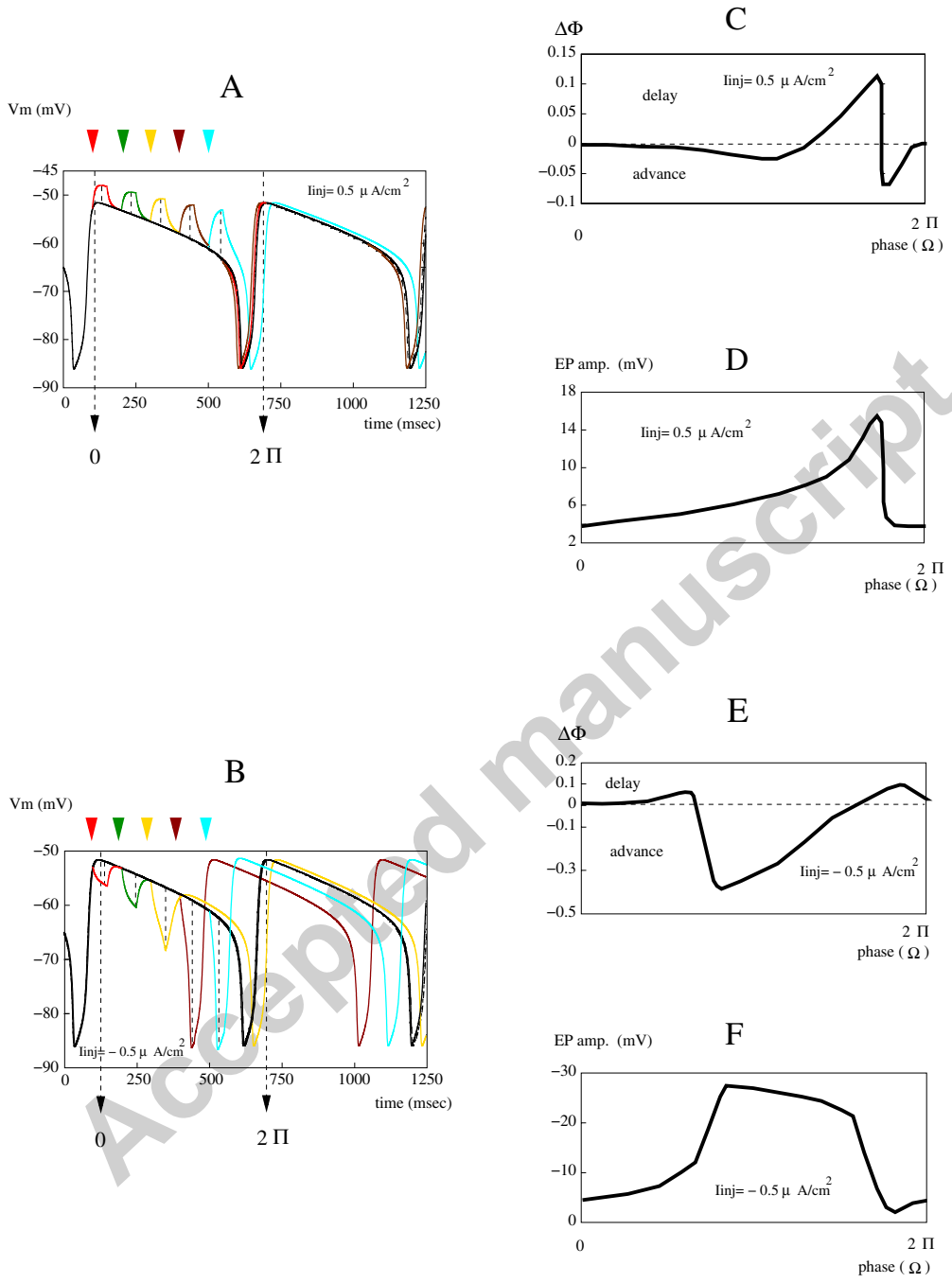

Fig. 8.

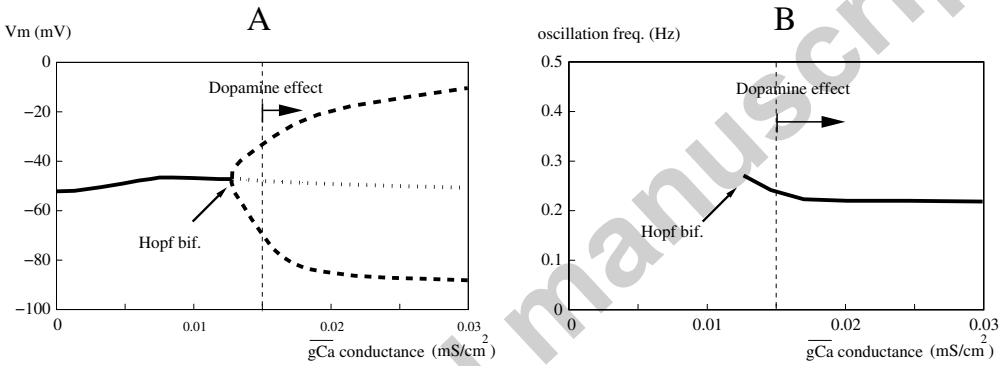

Fig. 9.